Optimizing the Synthesis Process of Wood-derived Biomorphic Silicon Carbide

by

Abdullah Yousef Alsalloum

Submitted to the Department of Materials Science and Engineering
in Partial Fulfillment of the Requirements for the degree of
Bachelors of Science in Materials Science and Engineering

at the

Massachusetts Institute of Technology

June 2017

Signature of Author... Signature redacted .....

Department of Materials Science and Engineering
April 29, 2016

Certified by..... Signature redacted .....

Michael J. Tarkanian,
Department of Materials Science and Engineering
Thesis Supervisor

Accepted by..... Signature redacted .....

Geoffrey S. D. Beach,
Professor of Materials Science and Engineering
Chairman, Undergraduate Thesis Committee

Optimizing the Synthesis Process of Wood-derived Biomorphic Silicon Carbide

by

Abdullah Yousef Alsalloum

Submitted to the Department of Materials Science and Engineering
in Partial Fulfillment of the Requirements for the degree of
Bachelors of Science in Materials Science and Engineering

Abstract

Biomorphic silicon carbide, a porous, light and high strength ceramic typically derived from natural wood, has great potential in high temperature and structural applications. Over the past several years, researchers have developed three main routes to fabricating biomorphic SiC: reactive infiltration of molten Si, chemical vapor infiltration of Si or SiO, and SiO_2-bearing solution infiltration. In this study, the latter was investigated and optimized. In addition, a novel synthesis technique, Si suspension infiltration, is proposed that overcomes the major issues present in the current methods. Four wood species (balsa, pine, maple and oak) offering a wide range of porosities were infiltrated with colloidal SiO_2 under varying pressure conditions, and the corresponding weight gains were recorded and studied. The samples were then fired at 1600 °C for 2h under argon flow, and examined via X-ray diffraction (XRD), scanning electron microscopy (SEM) and compression testing. It was found that applying pressure or vacuum produced more effective SiO_2 weight gains. Pine showed superior absorption to other types with its maximum obtained value achieved under vacuum followed by pressure. The starting concentration of SiO_2 solution proved to be crucial in controlling the final mechanical properties of the specimens. XRD analysis revealed that the resulting samples consisted of nearly pure SiC, and SEM images indicated that the initial structure of wood was retained. Due to the nature of the reactions involved with using SiO_2 as a precursor, the produced specimens tend to be mechanically weak. The new synthesis approach involves the use of <10 μm sized particles of Si instead of nano-sized SiO_2 particles. Pine was selected to serve as the template for absorption, and after two infiltration treatments, the sample absorbed 55.6% of its weight, ~4% higher than its theoretical stoichiometric need, 51.3%. EDS analysis revealed that Si was able to spread homogenously, and XRD spectra confirmed the material identity to be composed of mainly pure SiC with minor trace metal contamination. Compression testing illustrated better mechanical properties of the Si prepared specimen, suggesting the potential of this method to replace existing techniques.

Acknowledgements

I would like to thank:

- Mike Tarkanian, my thesis advisor, who provided valuable guidance and support whenever needed, and for holding weekly meetings to ensure that my thesis proceeded as smoothly as possible.
- Shaymus Hudson for providing workspace, access to equipment (tube furnace, vacuum chamber, pressure tank ...etc.), and spending some time training me on these devices.
- Charlie Settens for helping with XRD training and technical difficulties.
- Patrick Dixon for his help in performing compression testing and for providing balsa wood.
- Don Galler for SEM and EDS training and answering technical questions.
- Bonnie Wang, Harry Thaman and Nagisa Tadjfar for encouraging me to continue on with this topic and try to advance new findings.
- MIT's Department of Materials Science and Engineering for offering the opportunity to engage in research and for clearly articulating the thesis requirements.

Table of Contents

List of Figures

List of Tables

1. Introduction and Motivation

Porous materials carry unique properties that are usually not observed in their dense form. These properties include lower density, higher surface area, higher specific strength, lower thermal conductivity and controlled permeability all resulting from the presence of voids replacing solid material.[1] Thus, cellular materials are found in a wide range of applications including energy absorption, lightweight structures for buildings and airplanes, filtration devices, and bone substitution materials.[1,2]

Unlike porous metals and polymers, cellular ceramics tend to be more brittle and have therefore been traditionally avoided.[1,3] Nevertheless, they possess unique properties that make them suitable for multiple emerging applications. Porous silicon carbide (SiC) ceramics have attracted a great deal of research in the field of porous materials due to their unique combination of properties including high melting point (2700 °C), outstanding corrosion resistance, high thermal conductivity and excellent mechanical properties.[4–6] Porous SiC is considered as one of the best material candidates for hot gas filters, molten metal filtration, diesel particulate filters, dental implants, catalytic supports, acoustic and thermal insulation, and composite reinforcements.[7,8]

Biomorphic SiC ceramics are a new class of materials that are produced via biotemplating, which is simply the use of a biological substance as a template for a synthetic one.[5] Biological structures have been of great interest recently due to their inherent hierarchical design, which has been optimized during the process of evolution.[4] Wood is the most commonly used template for biomorphic ceramics mainly due to its open porous system of tubular cells and its high mechanical strength to weight ratio.[5,7] In addition, its many different species offer a wide range of densities and microstructures to

choose from depending on the application in hand. Wood consists of cellulose (~50%), hemicellulose (~25%), and lignin (~25%). These percentages vary depending on the typed of wood used.[9]

There are some advantages for using the biomorphic SiC technique over others such as sintering and reaction-bonding. Sintering approaches consume a significant amount of energy by requiring temperatures of around 2000 °C and SiC powder as a starting material.[10] Reaction-bonding utilizes a lower sintering temperature but requires the addition of bonding agents, which lower the thermal conductivity and degrade the mechanical properties of the resulting component.[7] Both of these techniques often yield relatively low porosities (<%60 vol).[1] On the other hand, wood-derived biomorphic SiC is energy efficient, as it involves lower processing temperatures, does not require high-purity starting powders, and makes use of a renewable resource, wood.[11] Also, no additives or bonding agents are necessary. Finally, wood microstructures are replicated offering a wide variety of microstructures available with excellent mechanical properties. At a porosity range of 50 - 80%, wood-derived biomorphic SiC ceramics show higher strength than that produced by other techniques.[7] Arellano-López et. al. argue that production of biomorphic SiC is easier to industrialize compared to other advanced ceramics, which normally require a high degree of technological improvement and well qualified and skilled human resources.[5]

There are currently three main methods for synthesizing biomorphic SiC from wood precursors, but all involve the following two major steps.[12] First, wood is pyrolyzed at high temperatures under inert gas flow to produce amorphous carbon and volatile sub-products. Depending on the wood type, pyrolysis starts at around ~200 °C and

decomposition is completed at ~500 °C.[13] Second, at high temperatures (~1600 °C), a silicon-bearing compound reacts with the carbon template to produce SiC. The silicon-bearing compound comes in different forms depending on the method used.

The first method is the reactive infiltration of molten Si where pyrolyzed specimens are mixed with Si powder, put in a vacuum furnace at a high temperature, and infiltrated with molten Si.[9,11,13–22] While this method leads to mechanically robust samples, excess Si of up to 100% more than the stoichiometric ratio is needed to ensure complete conversion to SiC.[21] Excess free silicon not only reduces the porosity, but also limits the application temperature and corrosion resistance due to the melting point of silicon (~1400 °C) and its ability to oxidize. To make use of the porosity of the specimens, the excess silicon needs to be etched out by soaking in a mixture of hydrofluoric acid (HF) and nitric acid (HNO_3), which is an expensive process dealing with extremely corrosive and toxic acids.[9,10,14,23–27] In addition, silicon is wasted escaping the reactions as silicon tetrafluoride (SiF_4), a poisonous and possibly fatal gas if inhaled.[28] To completely remove excess silicon, long soaking times are needed. According to Torres-Raya et. al., the etching process is diffusion limited, and successful removal of residual Si took more than 64 hrs.[29] A significant drop in mechanical strength was observed after the etching process. This approach also demands an evacuated environment to allow infiltration and diffusion of the melt through the sample pores.

The second method is the chemical vapor infiltration technique (CVI) or the reactive infiltration of Si or SiO gas.[8,30–36] Residual silicon clogging pores is greatly reduced in this case. Vogli found that the gas phase reaction resulted in clogging of significantly smaller pores when compared with the liquid silicon infiltration method.[33]

However, this technique is limited to template thicknesses of less than 10 mm.[33,37] Moreover, to achieve complete conversion to SiC, holding times of more than 15 hours at high temperatures are needed, which is energy intensive. According to Vogli, full conversion of a 10 mm thick sample was achieved after holding at 1600 °C for more than 16 hrs.[33]

The third method is the infiltration of wood with an SiO_2-containing solution before firing at high temperatures.[12,37–45] The most commonly used SiO_2 precursor is tetraethyl orthosilicate (TEOS), where gelation of SiO_2 occurs according to the sol-gel process.[12,38,42,43,45] Others have also used sodium silicate (Na_2SiO_3) as the SiO_2 precursor.[44,46] Of the three methods, this is the most efficient and economical according to Qian.[39] Highly pure and porous samples with no excess silica are obtained. The size of the specimens is not limited to 10mm, and a vacuum furnace is unnecessary. Instead, conversion occurs under argon flow, which allows the pyrolysis and SiC conversion steps in the silicon melt approach to be combined into one step inside one furnace. The main disadvantage of this method is that due to the various destructive reactions involved with using SiO_2 instead of Si, which will be discussed in more detail later, the resulting specimens experience weaker mechanical properties.[8]

In this thesis, the SiO_2 infiltration method is employed and optimized using colloidal silica, which is a fine dispersion of amorphous silica nanoparticles in a liquid. This choice of solution brings certain advantages over the use of TEOS or Na_2SiO_3 (discussed under Materials and Methods). The parameters optimized are the starting solution, wood type, synthesis time, infiltration pressure and silica concentration. Temperature optimization

has been investigated previously and a firing temperature of 1600 °C was found optimal for complete conversion to SiC.[39,43]

In addition, a novel synthesis route is proposed that overcomes all of the aforementioned issues. Wood is infiltrated with a suspension of $<10\ \mu m$ Si particles, instead of a suspension of ~22 nm SiO_2 particles. The macro size pores of the wood allow the Si particles to enter, and full conversion to SiC was attained at 1600 °C for 2 hours holding time. Compared with the Si melt approach, this method eliminates the need to use excess Si and to undergo the expensive etching process. With nearly the same theoretical stoichiometric ratio, full conversion of the sample was achieved. Compared with the CVI technique, much shorter holding times were required for successful conversion. Finally compared with the SiO_2 method, the carbothermal reducing reactions weakening the mechanical properties of the resulting specimens no longer take place.

2. Materials and Methods

2.1 Material Preparation and Controlled Parameters

2.1.1 Starting materials

To incorporate a wide spectrum of densities and microstructures, 4 types of wood (2 softwoods and 2 hardwoods) were used. Softwoods were pine and balsa with physical porosities 76% and 89% respectively. Hardwoods were maple and oak with porosities 56% and 50% respectively. Using a band saw, the wood samples were cut to the following dimensions: 25 x 25 x 5 mm for pine and balsa, and 25mm diameter x 5 mm height for maple and oak (Figure 1). The specimens were dried at 100 °C to a constant weight.

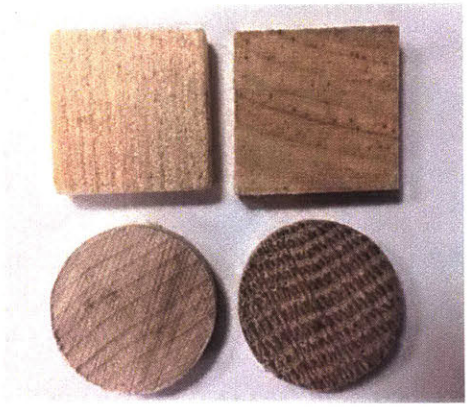

Figure 1: 25X25X5 mm balsa (left) and pine (right), and 25mm diam. X5mm maple(left) and oak(right).

A 50% weight colloidal silica suspension in water (LUDOX® TM-50, Sigma-Aldrich) of particle size 22 nm served as the SiO_2 precursor. Varying the concentration was performed by diluting the solution to the desired weight percentage. Colloidal silica is a more efficient, safer and cheaper option than dealing with TEOS or sodium silicate. To hydrolyze TEOS to silica, adding HCl, ethanol and water are required. Different molar ratios of each produce different particle sizes, acidities, SiO_2 concentrations and viscosities that may be difficult to control, stabilize and reproduce.[47,48] This extra processing step increases the overall synthesis time. Likewise, for sodium silicate, an HCl treatment is necessary to neutralize the solution.[44] In addition, the viscosity of sodium silicate is high and becomes higher as the concentration increases, which may affect the infiltration rate of the solution through the wood pores.[49] In terms of safety, TEOS is a highly flammable liquid that may cause serious eye and respiratory irritations, while sodium silicate is a highly corrosive basic (pH = 12) solution that is damaging in case of skin contact.[50,51] On the other hand, colloidal silica has a pH of 9 and a viscosity close to that of water even at high silica concentrations (~50%). It is safe, environmentally-friendly

and does not require the extra step of mixing with HCl, which saves effort and processing time.[52]

Si powder of particle size 45 microns (~325 mesh, 99% trace metals basis, Sigma-Aldrich) was ball milled to particle size less than 10 microns, and a solution of 33% weight Si was prepared by adding the powder to DI water. The Si powder did not oxidize to SiO_2 in the process, which was confirmed by the absence of oxygen via EDS.

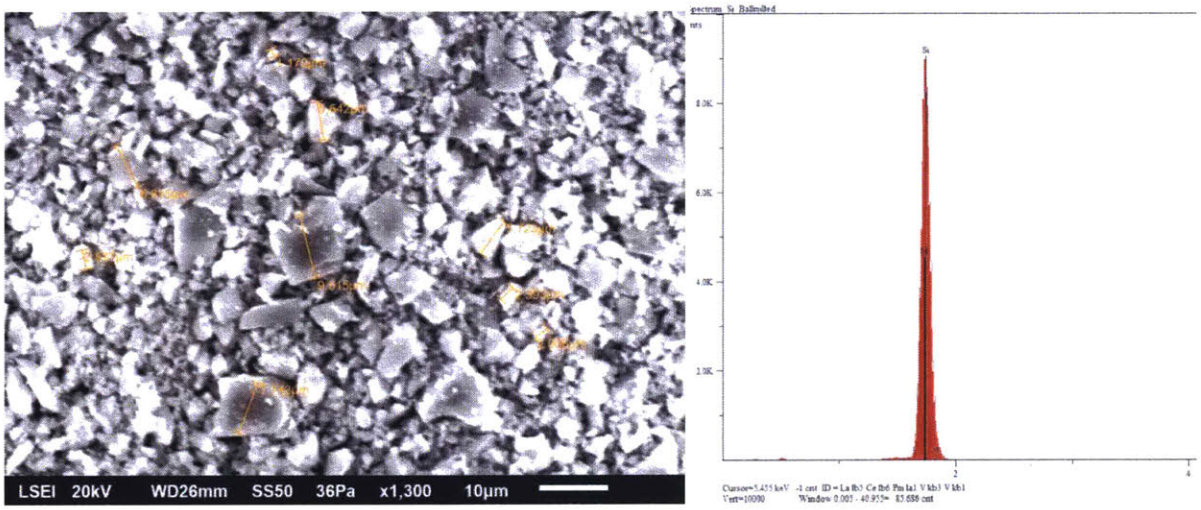

Figure 2: SEM image of ball milled Si powder of size less than 10 microns (left), and corresponding EDS spectrum identifying the powder to consist of mainly elemental Si (right)

2.1.2 Infiltration

Wood pieces were soaked in colloidal silica under four different settings: no applied pressure, pressure, vacuum and combination of vacuum then pressure. Pressurizing and evacuating the solutions were performed in a pressure tank and vacuum chamber respectively (Figure 3). The main goal was to maximize absorption. To test the relationship between pressure and absorption, applied pressure was varied from 0 psi (atmospheric pressure) to 55 psi, while the vacuum pressure was held constant at

approximately -13 psi. The wood specimens were dried at 100 °C for 2 hours and the corresponding weight gains due to the SiO_2 uptake were measured. Wood type and pressure conditions that yielded highest absorption were considered for Si infiltration method.

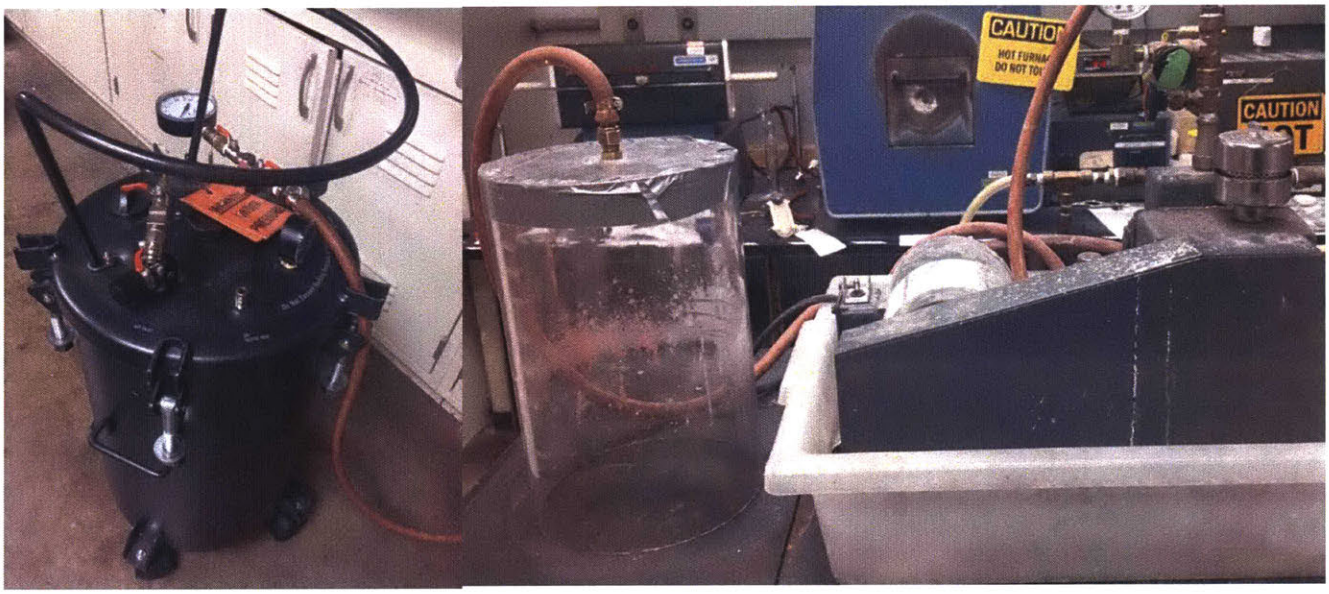

Figure 3: Pressure tank (left), and vacuum chamber along with vacuum pump (right).

2.1.3 Pyrolysis and Ceramization

After infiltration, the samples were placed on alumina boats in a tube furnace under argon flow at a rate of 15 scfh (Figure 4). The temperature was held at 1600 °C for 2 hrs with a heating ramp of 5 C/min. In addition, non-infiltrated wood pieces were fired to see the effect of pyrolysis on weight loss and dimensions of the specimens.

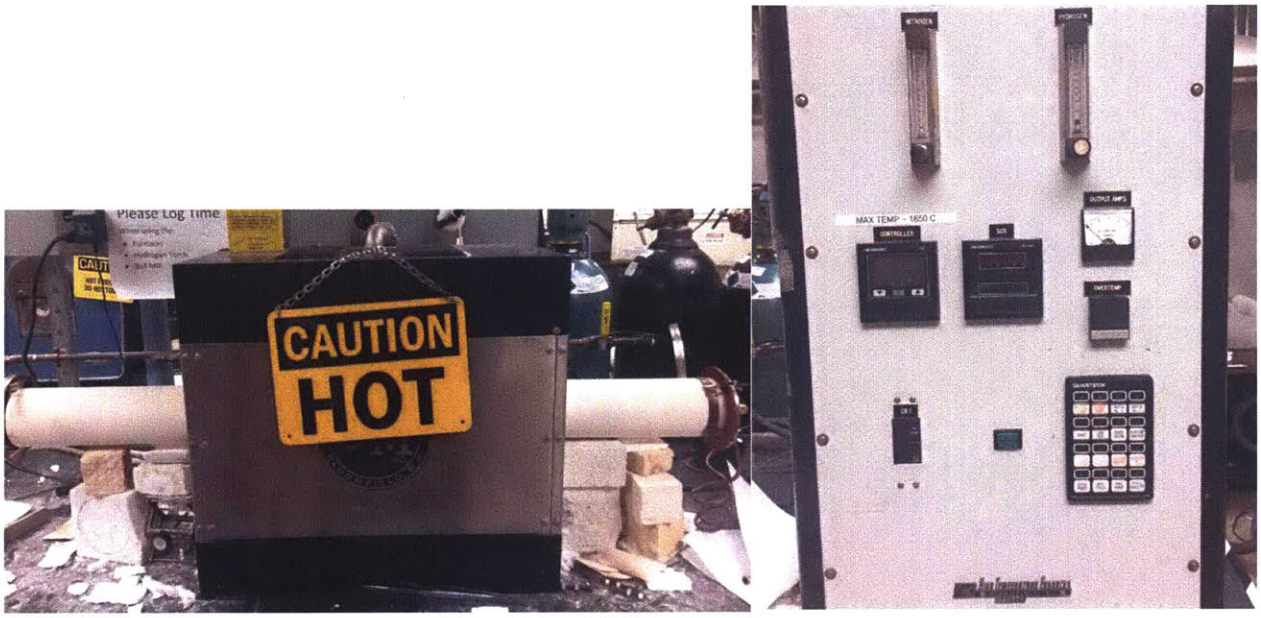

Figure 4: Alumina tube furnace (left), and setup panel including temperature and flow controllers (right).

Conversion to SiC occurs according to the following reaction when SiO_2 is used as the precursor:

$$SiO_2 + 3C \rightarrow SiC + 2CO \quad (1)$$

This reaction proceeds in two steps:

$$SiO_2 + C \rightarrow SiO + 2CO \quad (2)$$

$$SiO + 2C \rightarrow SiC + CO \quad (3)$$

When Si is used, the reaction proceeds as follows:

$$Si_{(l)} + C_{(s)} \rightarrow SiC_{(s)} \quad (4)$$

Reaction 1 shows that a molar stoichiometric ratio of 1:3 of silica to carbon is needed, which translates to about 34% weight gain of the original wood pieces. Reaction 2

requires more silicon uptake as the stoichiometric ratio of silicon to silica is 1:1. Specifically, a ~50% weight gain is necessary for full conversion.

2.2 Characterization

2.2.1 Weight Loss and Dimension Change after Pyrolysis

To determine the weight loss due to pyrolysis, two non-infiltrated pieces of each type of wood were weighed before and after firing. The loss percentage is given by:

$$\%\, weight\ loss = \frac{W_{wood} - W_{charcoal}}{W_{wood}} * 100$$

Likewise, the shrinkage in axial and radial directions were found by measuring the dimensions with a caliper before and after pyrolysis according to the equation:

$$\%\, axial, radial\ shrinkage = \frac{dim_{before} - dim_{after}}{dim_{before}} * 100$$

2.2.2 Percent Free Carbon

The presence or absence of free carbon in the SiC specimens was detected by heating in air at 700 °C for 2 hours and weighing the samples before and after the treatment. Unreacted carbon was calculated as follows:

$$\%\, free\ carbon = \frac{W_{before} - W_{after}}{W_{before}} * 100$$

2.2.3 Physical Porosity Measurements

Density was found by dividing the mass by the geometric volume, and physical porosity was determined according to the equation:

$$\%\, porosity = \left(1 - \frac{\rho_{specimen}}{\rho_{cell\ wall}}\right) * 100$$

where ρ here represents density

According to Gibson, the wood cell wall density has a standard value of 1500 kg/m^3, representative of cellulose fibers, hemicellulose and lignin.[53]

2.2.3 X-ray Diffraction

XRD spectroscopy was conducted on the SiC samples using a Rigaku diffractometer with Cu-Kα (λ = 1.5418 Å) radiation at 45 kV and 200 mA (Figure 5). XRD provides information regarding the identity, purity and crystallinity of the material.

Figure 5: Rigaku SmartLab X-ray diffractometer

2.2.4 Scanning Electron Microscopy (SEM) and Energy-dispersive X-ray spectroscopy (EDS)

JEOL JSM 6610LV SEM equipped with EDS was used to observe the morphological and elemental features of the samples. High vacuum environment was

carried out for SiC specimens, while low vacuum mode was applied for wood to prevent charging of the non-conductive material.

2.2.5 Compression Testing

The mechanical behavior of the SiC samples was investigated using an Instron 4201 Compression Tester (Figure 6). Compression was performed in the axial direction at a constant strain rate of 0.1 mm/min using a 500 N load cell.

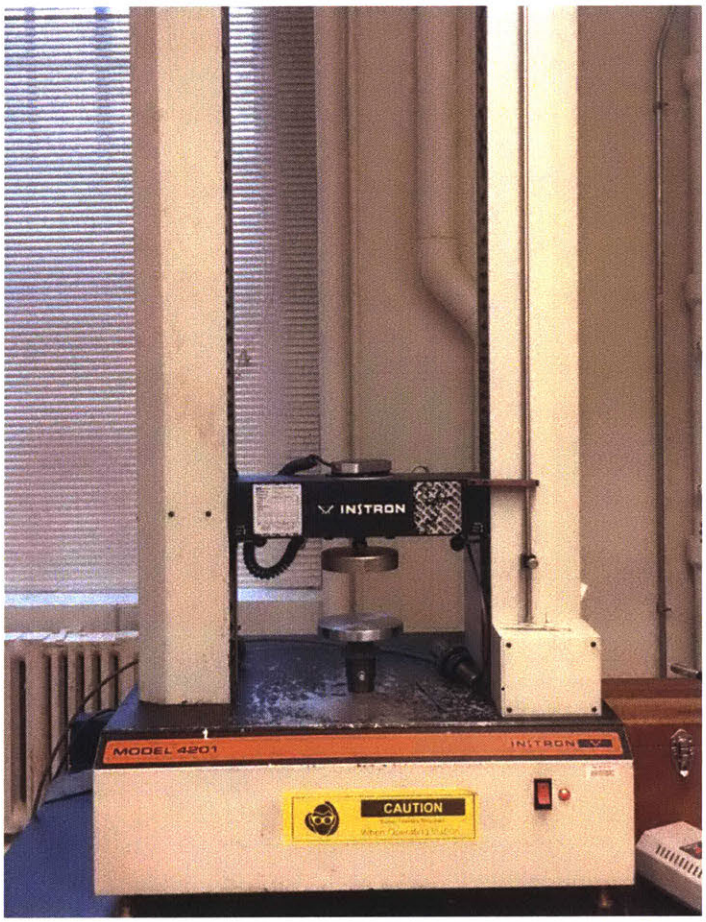

Figure 6: Instron 4201 with a 500N load cell for compression testing.

3. Results and Discussion

3.1 Weight Loss and Dimension Change after Pyrolysis

Table 1 shows the effect of pyrolysis on weight loss for various wood types. Regardless of the type, the decrease in weight lies approximately between 77-78%. This result agrees well with literature values. Sinha et. al. found that the typical proximate analysis of dry wood by %weight is about 77% volatile matter.[54] According to Sinha, the resulting material consists of about 20% fixed carbon and 3% ash for hardwoods, and about 22% fixed carbon and 1.5% for softwoods.[54] This information combined with that of reactions 1 and 4 above allows us to determine the theoretical weight gain needed for wood to fully convert to SiC, which is estimated to be 33.3% for hardwoods and 36.6% for softwoods.

Wood Type	piece no.	mass before(g)	mass after(g)	**%weight loss**
Balsa	1	0.200	0.044	**78.044**
	2	0.198	0.045	**77.307**
Pine	1	0.980	0.220	**77.544**
	2	0.988	0.228	**76.916**
Maple	1	1.676	0.366	**78.168**
	2	1.681	0.372	**77.858**
Oak	1	1.856	0.412	**77.788**
	2	1.826	0.403	**77.917**

Table 1: Percent weight loss due to pyrolysis for two pieces of each wood type.

Table 2 below shows the shrinkage in both radial and tangential dimensions after pyrolysis. The results indicate that shrinkage ranges from 18% to 40%. For every specimen, contraction in the radial/tangential dimension is higher than in the axial one. These values are very similar to those obtained by Greil et. al.[14]

Wood Type	piece no.	Length (mm)	Width (mm)	Thickness (mm)	**% axial shrinkage**	**% radial/tangential shrinkage**
Balsa	1	18.55	18.65	3.85	**23.00**	**25.60**
	2	18.92	17.78	3.92	**21.60**	**26.60**
Pine	1	18.04	15.46	3.77	**24.60**	**33.00**
	2	18.42	14.86	3.81	**23.80**	**33.44**
		diam.1 (mm)	diam.2 (mm)	Thickness (mm)	**% axial shrinkage**	**% radial/tangential shrinkage**
Maple	1	16.55	14.51	3.96	**20.80**	**37.88**
	2	16.44	14.21	3.93	**21.40**	**38.70**
Oak	1	17.65	15.64	4.07	**18.60**	**33.42**
	2	17.48	15.6	4.09	**18.20**	**33.84**

Table 2: Percent shrinkage in the radial direction is greater than that in the axial direction.

3.2 Pressure and Weight Gain Analysis

Figure 7 illustrates the percent weight gain of the wood specimens as a function of applied pressure after the samples were infiltrated with 50% colloidal silica solution for 30 min and dried at 100 °C. It is important to note that the curves don't follow a very smooth curve, which is expected since each point comes from soaking a different cut of wood. In other words, a total of 7 pieces with the same dimensions were used to generate each plot. As shown, for balsa, maple and oak the %wt. gain increases significantly in the first 0-25 psi of applied pressure, and small changes are observed at higher pressures. For pine, the % wt. gain almost doubles after an application of only 5 psi and stabilizes with minor fluctuations above that value. The results might suggest that pressures in the order of 30-120 MPa (~4000 -17000 psi) as reported in literature may be unnecessary and expensive, yielding the same uptake as that at lower pressures.[12]

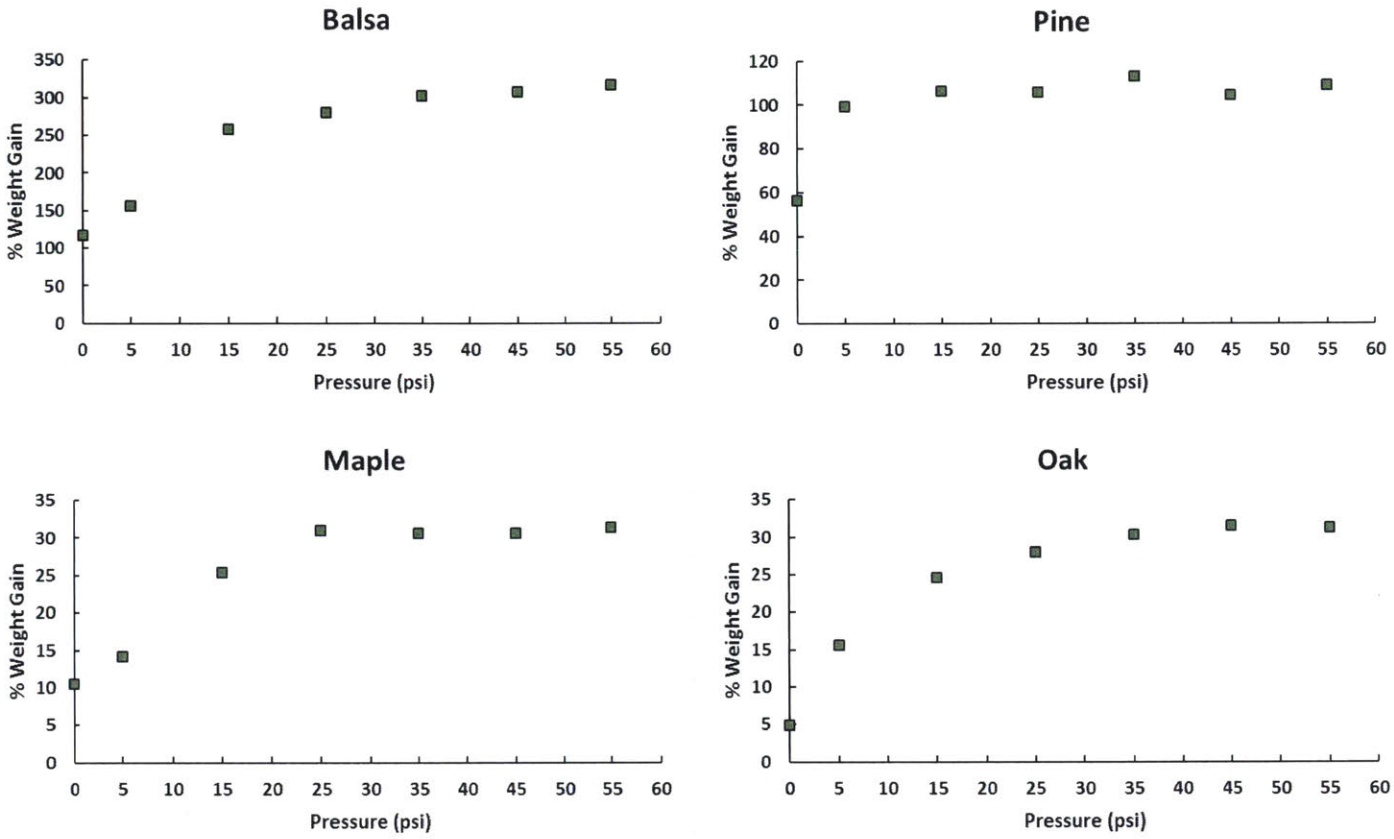

Figure 7: Percent weight gain as a function of applied pressure for balsa, pine, maple and oak.

Although balsa experiences the greatest percent increase in weight, it doesn't mean that it absorbed the most. Balsa's inherently light weight makes it very sensitive to changes in its percent weight gain. In fact, when considering the weight gain in grams, pine turns out to have gained the most SiO_2 even though its physical porosity is lower than that of balsa (Figure 8). The reason behind that is that pine has a much greater open porosity (accessible to external fluids) than that of balsa.

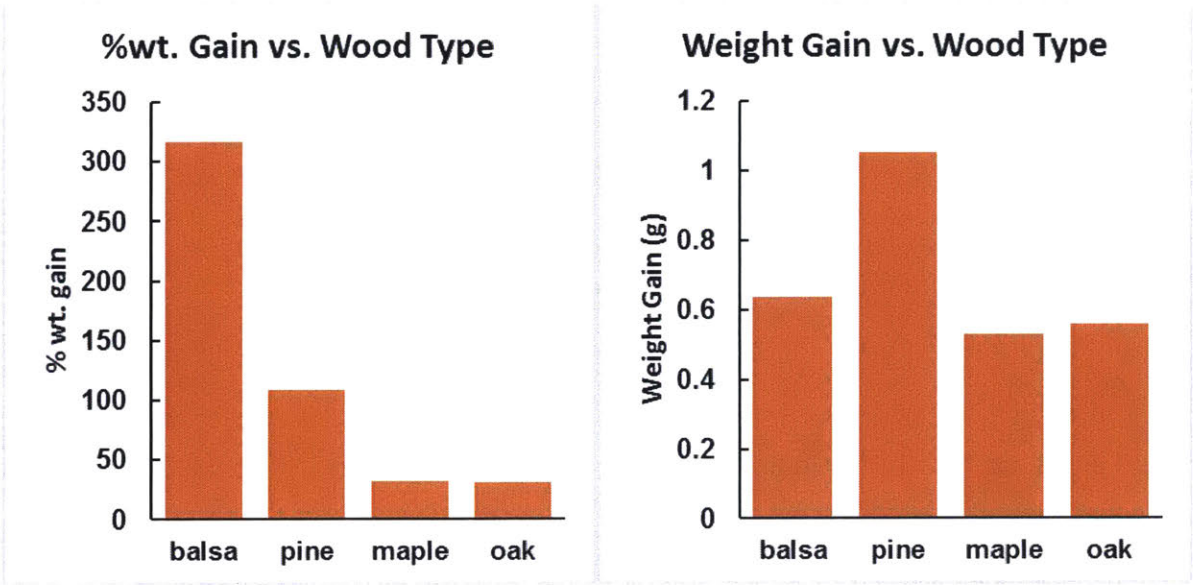

Figure 8: Percent weight gain at 55 psi for balsa, pine, maple and oak (left), and weight gain in grams at 50 psi for the same infiltrated pieces (right).

Figure 9 illustrates the effect of pressure and soaking time on the % wt. gain. Soaking at 55 psi for 30 min is compared to soaking at 0 psi for 30 min and 12 hrs. It is clear that for all wood types, the use of pressure is much more effective than leaving the samples to soak for long periods of time.

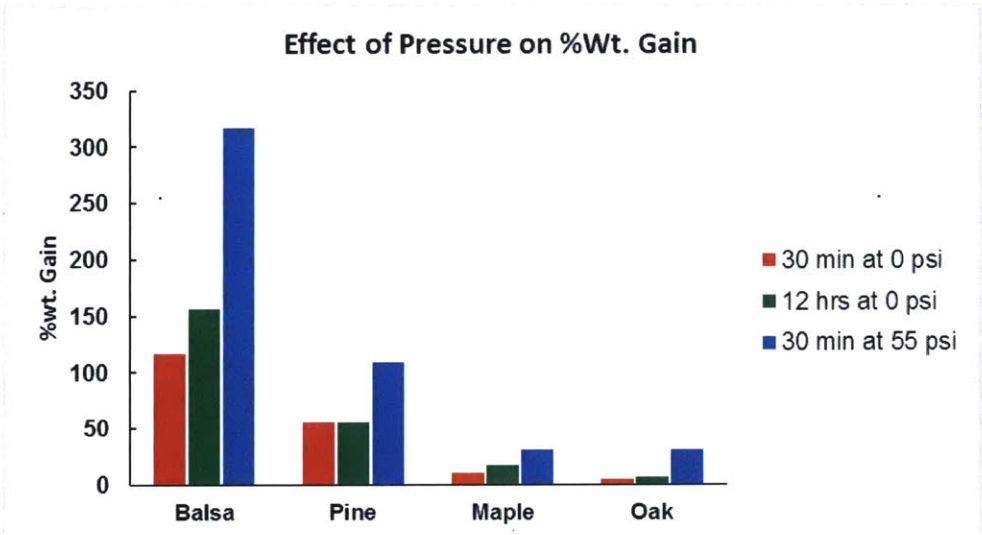

Figure 9: Percent weight gain for different soaking pressure and time conditions.

Figure 10 shows the effect of vacuum (-13 psi) on the %wt. gain of samples soaked for 30 min. The experiment was repeated with different wood pieces of the same dimensions to make sure the values obtained are not outliers. For balsa, maple and oak, the application of pressure seems to yield greater absorption when compared with vacuum. Surprisingly for pine, vacuum is more effective, resulting in a percent weight gain of ~140% as opposed to ~100% under pressure.

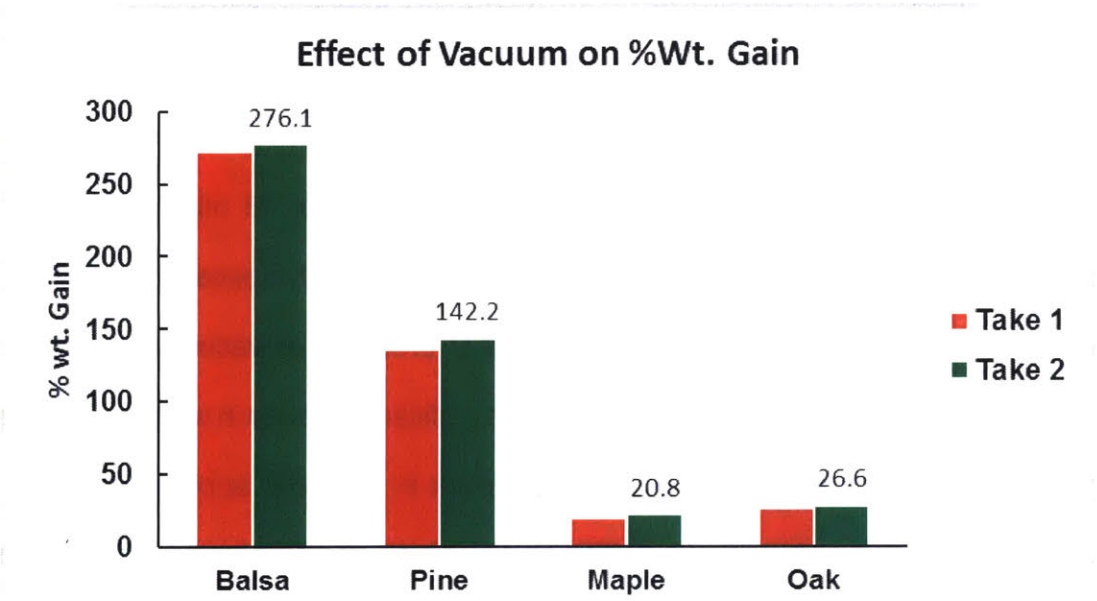

Figure 10: Percent weight gain at -13 psi or 30 min for two of each wood type.

Pine's exceptional behavior can be attributed to the presence of large amounts of air trapped inside it. This phenomenon was evident when observing the infiltration step under vacuum. A remarkable aggregate of bubbles left the solution and overflowed from the container (Figure 11). This large degree of bubbling was not observed in the other wood types. As a result, pine absorbed much of the solution under vacuum, whereas under pressure, the compressed air prevented the solution from being fully infiltrated.

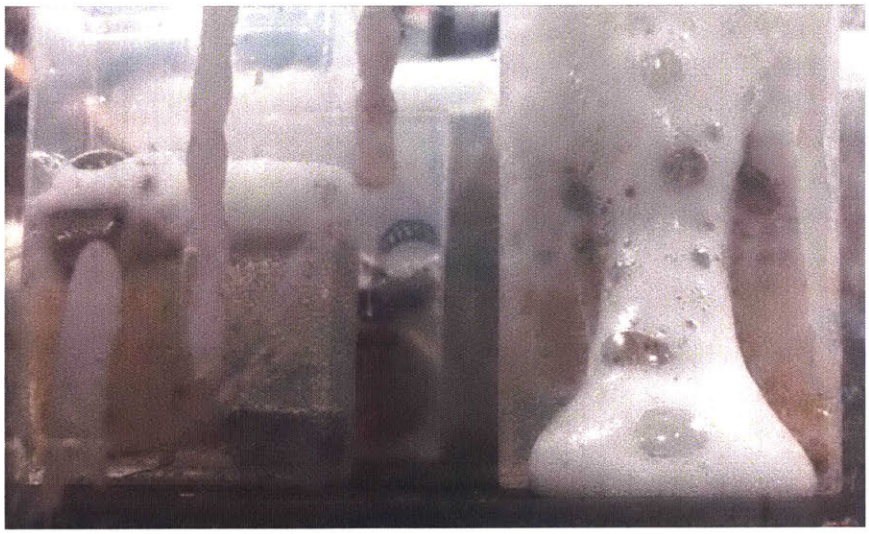

Figure 11: Significant amount of air leaving pine sample when soaking under vacuum (right) compared with balsa (left).

Finally, absorption was investigated under vacuum for 15 min followed by an applied pressure of 55 psi for another 15 min (Figure 12). With the exception of balsa, the %wt. gains are higher than those obtained under pressure or vacuum alone. Of the different wood types, pine experiences the most significant increase in weight. The reason why balsa didn't absorb as much was that it shrunk in size after applying pressure. Its weak structure couldn't handle the force exerted from extreme pressures. To test this shrinking effect, the procedure was repeated at pressures 35 psi and 15 psi. Indeed, for balsa, the higher the pressure, the more significant the contraction was (Figure 12). Moreover, the specimen infiltrated at 15 psi gained more SiO_2 weight than that at 55 psi due to its bigger size and thus, greater absorption capacity. This behavior was not observed in the other wood types.

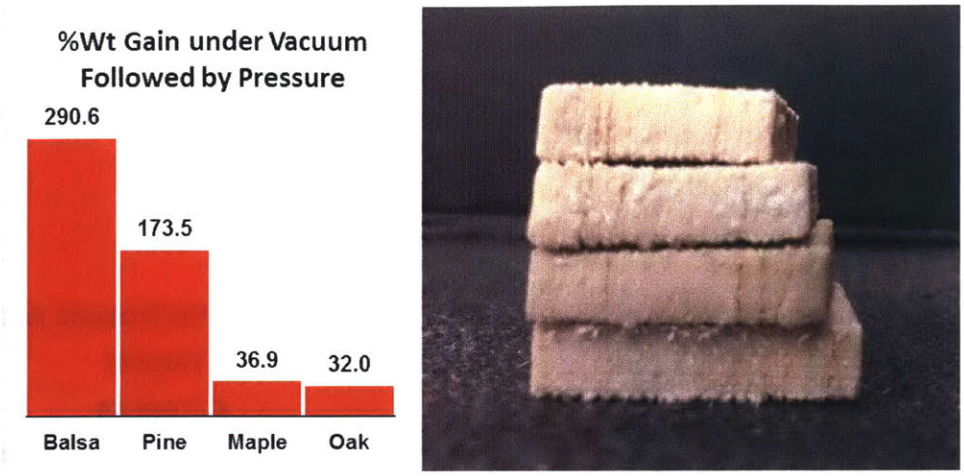

Figure 12: Percent weight gain under vacuum (-13 psi) for 15 min followed by pressure (55 psi) for 15 min (left). From top to bottom, balsa soaked at 55 psi, 35 psi, 15 psi and non-infiltrated (right).

Figure 13 summarizes the weight gain analysis under the four different pressure regimes: No applied pressure (30 min), pressure (55 psi for 30 min), vacuum (-13 psi for 30 min) and vacuum followed by pressure (-13 psi for 15 min, then 55 psi for 15 min (15 psi for balsa). There are a few conclusions to draw from this chart. First, the absence of pressure or vacuum results in inadequate weight gains, which may lead to non-homogenous solution absorption and incomplete conversion to SiC. Second, with the exception of pine, the use of pressure alone and vacuum followed by pressure yield roughly similar percent weight gains. Third, infiltrating pine under vacuum followed by pressure is much more effective than any of the other modes. Finally, since out of all the wood types, pine absorbed the most, it was chosen to test the new synthesis route, preparing SiC by infiltrating with a suspension of Si particles.

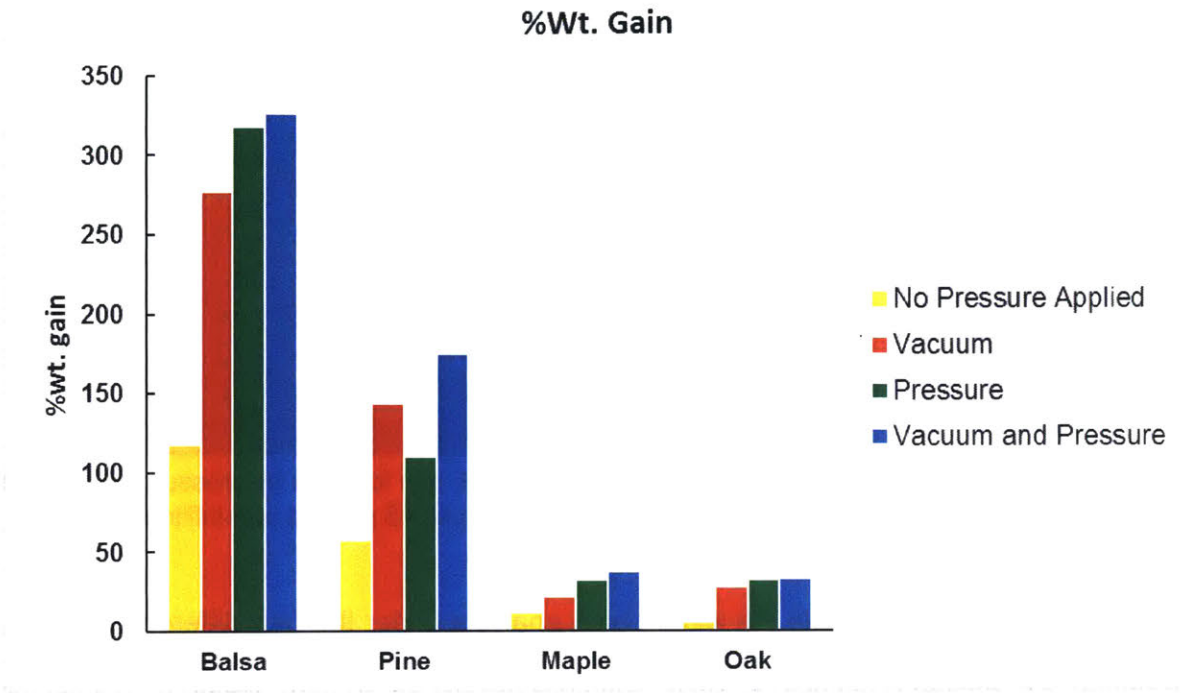

Figure 13: Percent weight gain for a total of 30 min soaking time under four pressure modes: atmospheric pressure, vacuum, pressure and vacuum followed by pressure

3.2 Effect of SiO_2 Concentration on SiC conversion

After firing the samples above that yielded greatest absorption, both balsa and pine specimens disintegrated, while maple and oak remained intact (Figure 14).

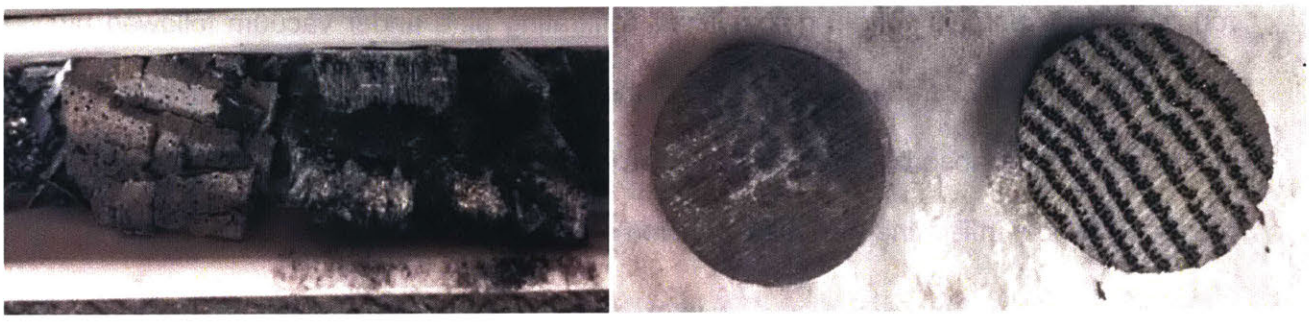

Figure 14: Biomorphic SiC samples after firing at 1600 °C for 2 hrs (From left to right: balsa, pine maple and oak). Balsa and pine with disintegrated, while maple and oak remained intact.

This unexpected result prompted the investigation of another reaction taking place, which was briefly discussed by Qian.[43] SiO_2 is capable of reacting with not only carbon, but also SiC according to the following reaction:

$$SiC_{(s)} + 2\,SiO_{2(s)} \rightarrow 3SiO_{(g)} + CO_{(g)} \quad (5)$$

The excess SiO_2 reacts with the SiC product and both are converted into gases. This in turn destroys the structure, causing the samples to disintegrate. This experiment indicates that the concentration of infiltrated SiO_2 solution matters; too much leads to a mechanically poor sample, while too little results in an incomplete SiC conversion. The stoichiometric percent weight gain needed is 36.6% for both balsa and pine and 33.3% for maple and oak. Since reaction 5 occurs as well, a higher percentage is necessary to achieve full conversion. Accordingly, the 50% colloidal SiO_2 solution was diluted to 12% for balsa and 15% for pine. The resulting weight gains after soaking under vacuum followed by pressure are 76.6% and 48.5% respectively. The two samples were then fired to see if this concentration would have any effect on the structure. Indeed, the produced specimens emerged whole and intact even when picking them up (Figure 15).

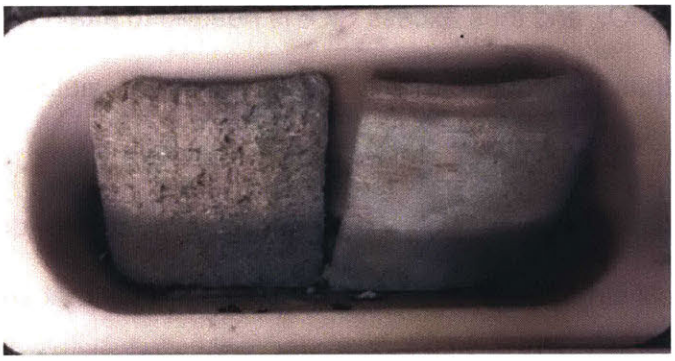

Figure 15: Balsa and pine specimens soaked at a lower concentration did not collapse and disintegrate after firing.

To determine whether complete transformation to SiC occurred or not, the SiC samples were heat treated in air and the percent free carbon lost was calculated according to equation 3. Table 3 below shows the initial %wt. gains of the wood pieces and the %wt. loss after burning off all the carbon.

Wood	%wt. SiO_2 Uptake	**%wt. Free Carbon**
Balsa	76.8	**-0.9**
Pine	48.6	**-0.2**
Maple	36.9	**18.5**
Oak	32.0	**42.3**

Table 3: Percent weight free carbon after burning off excess carbon at 700 °C for 2 h.

The values suggest that both pine and balsa successfully converted to SiC. The slight weight increase is due to the formation of a protective SiO_2 layer as reported by others. The oxidation reaction proceeds as follows:

$$SiC_{(s)} + \frac{3}{2}O_{2(g)} \rightarrow SiO_{2(s)} + CO_{(g)} \quad (6)$$

Although Maple absorbed more than its theoretically needed uptake by ~3%, 18% of the specimen was still unreacted carbon. This indicates that reaction 5 was taking place, the SiC was reducing the SiO_2, and thus excess SiO_2 is needed to attain full conversion. Oak absorbed ~1% less than its required stoichiometric ratio, yet, yielded a carbon weight percentage of 42.3%, meaning that almost half the sample didn't react. The reason behind the large discrepancy between oak and maple is the difference in their microstructure. Maple's structure is diffuse-porous having pores that are distributed fairly evenly. Oak, on the other hand, has a ring-porous structure with the largest pores concentrated in the early-wood. Oak's bimodal structure results in an uneven uptake of

SiO_2, which disrupts carbon to SiO_2 ratios necessary for the successful flow of the reactions. The large-pores region experiences complete conversion to SiC; however, excess silica exists and thus, more of reaction 5 is occurring. The small-pores or the late-wood region is short of SiO_2, which leaves the sample with unreacted carbon. One can observe Oak's large vessels becoming more prominent and even joining after firing (Figure 14). This non-homogenous absorption of oak makes it a poor candidate for synthesizing biomorphic SiC from SiO_2 precursors. It is important to note that the oak specimen fell apart after burning off excess carbon.

3.3 Absorption of Si Particles and SiC Formation

Si uptake of pine infiltrated with the Si solution under vacuum for 15 min followed by 55 psi for 15 min is shown in Figure 16. Unlike the previous method, the weight gain here is much less (~38% as opposed to ~174%) which is expected for two reasons. First, the concentration of Si in the suspension is 33.3% compared with 50% SiO_2. Second, the particle size of Si is ~150 times bigger than that of SiO_2, and therefore, particles are blocked by the smaller pores in the wood. The premise is that when the temperature exceeds the melting point of Si (~1400 °C), the melt will be able to penetrate these small pores. Pine requires a theoretical weight gain of ~51.3% to fully convert to SiC. However, only 38% was attained. To solve this problem, either a higher starting concentration can be used, or multiple treatments can be conducted. The latter was employed and with the second treatment, a %wt. gain of 55.6% was achieved, which is ~4% above the stoichiometric need. In this case, reaction 4 occurs and Si doesn't react with SiC as is the case with SiO_2. Therefore, 55.6% might be adequate for full transformation to SiC.

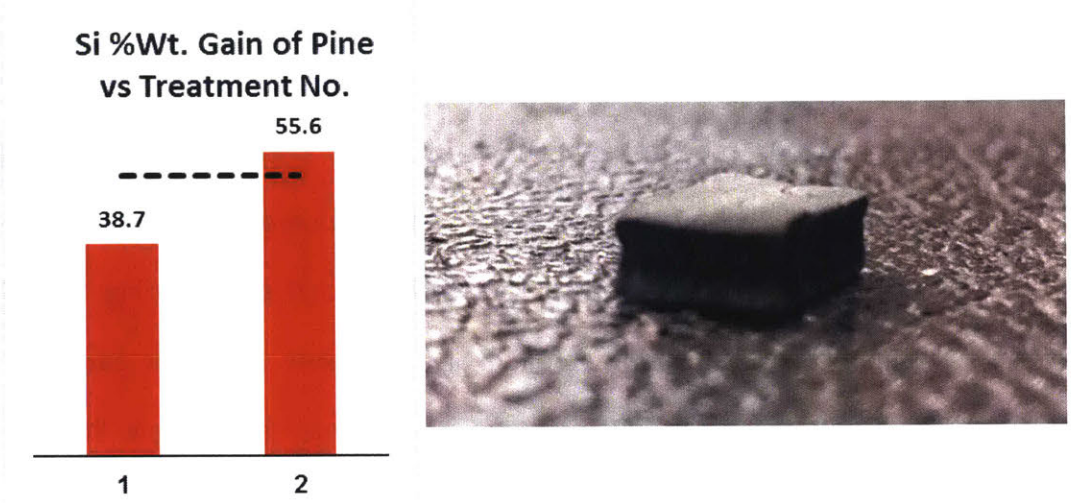

Figure 16: Percent weight gain of pine after soaking in Si suspension under vacuum followed by pressure attained its required uptake after 2 treatments (left). Sample after firing (right).

After firing, the sample emerged intact; however, its sides were slightly curved inwards (Figure 16). The reason behind this deformation is unknown, but it is believed that the force exerted on the surface pores by the Si powder after being pressurized inside caused the top and bottom surfaces to somewhat enlarge during the pyrolysis step. This defect may affect the mechanical properties of the resulting specimen. A solution to that would be to try using vacuum solely, or infiltrating with Si after pyrolyzing wood as practiced by others.

To investigate conversion efficiency, the sample was heat treated in air and the percent free carbon was determined according to equation 3. A weight loss of -0.74% was achieved, meaning that the sample gained a little due to reaction 6 taking place. This indicates that the specimen completely converted from amorphous carbon to SiC.

3.4 XRD Analysis

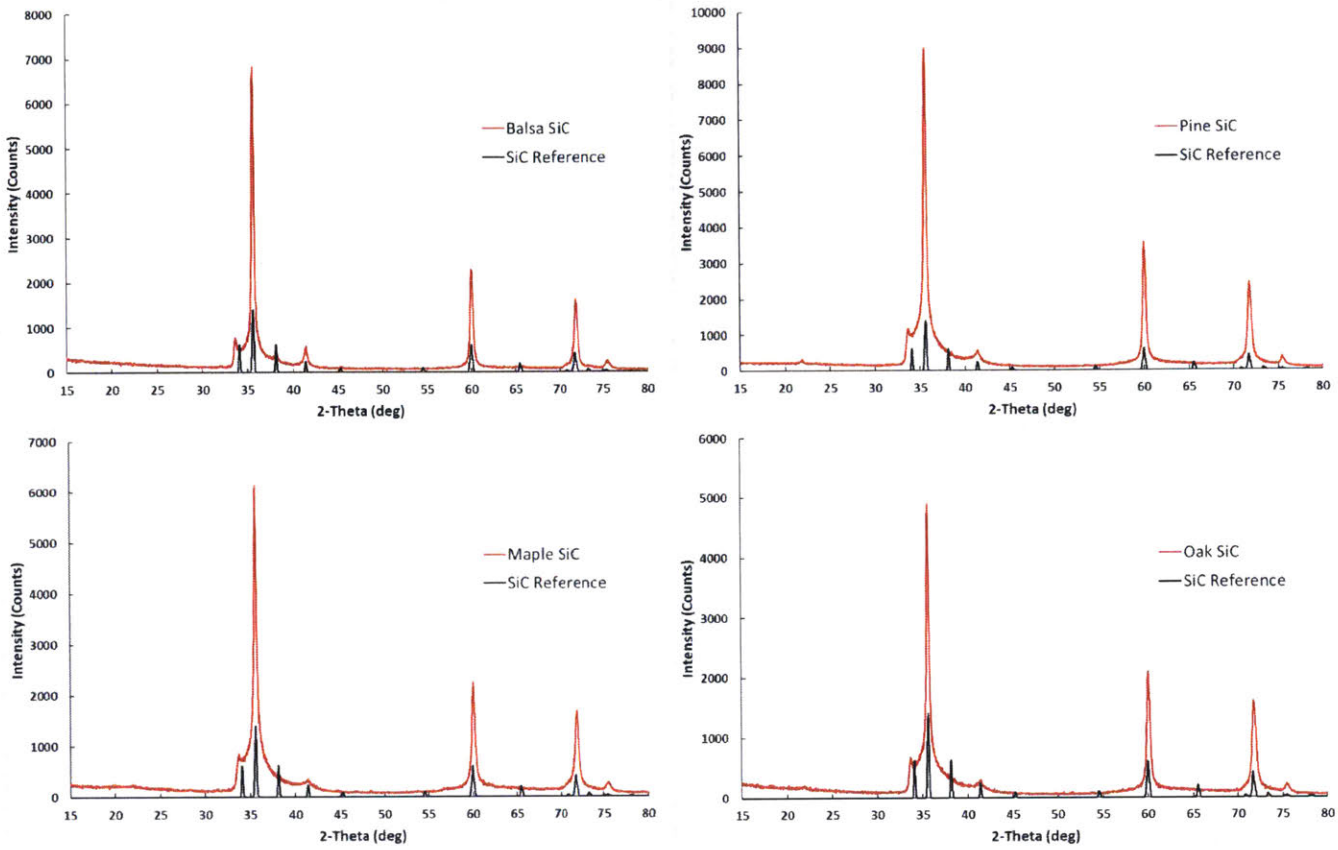

Figure 17: XRD spectra of samples prepared from colloidal SiO_2 show nearly pure SiC

Figure 17 shows the XRD plots of the biomorphic SiC samples prepared from colloidal SiO_2. The spectra match that of the reference SiC pattern indicating that the specimens consist of mainly pure SiC. Recall that balsa absorbed silica equivalent to 76.8% of its weight, more than twice of the required theoretical weight percentage. Yet no SiO_2 or, more specifically, cristobalite peaks are present. Cristobalite is phase of SiO_2 that forms at high temperatures and is reported by others to develop at ~1600 °C. Its main diffraction peak occurs at an angle of 22°, and tiny ones can be seen in the spectra of pine, maple and oak. HighScore Plus Analysis software calculates the amount of SiO_2 in these samples to be much less than 1 at%. While the balsa specimen is composed of

pure SiC, the fact that no SiO_2 peaks exist provides more evidence supporting the occurrence of reaction 5, which ultimately works on weakening the sample.

Figure 18 illustrates the spectrum for biomorphic SiC obtained from infiltrating pine with Si particles and firing at 1600 °C for 2 hrs. The peaks match that of the reference SiC pattern indicating the purity of the sample. There exist very small peaks before 35°, which can be due to contamination resulting from trace metals present in the starting Si powder or the ball milling media and container. Note that there are no Si or SiO_2 peaks perceived, suggesting that Si fully reacted with the amorphous carbon.

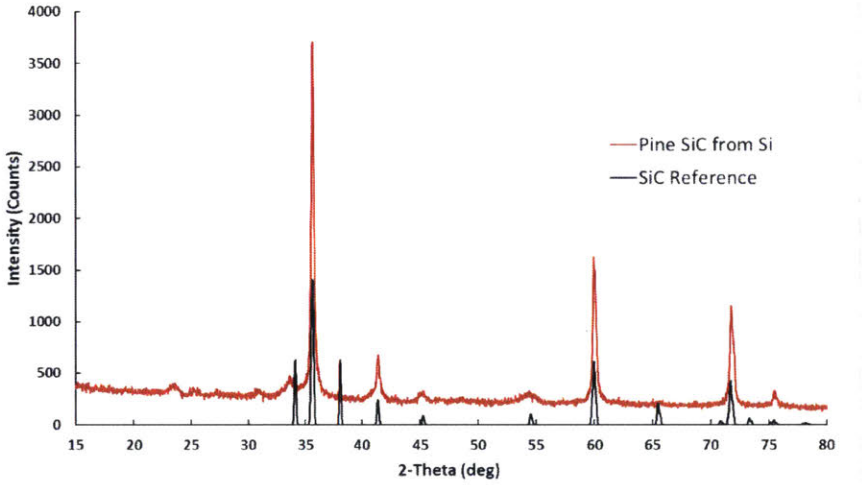

Figure 18: XRD spectrum of specimen prepared by infiltrating with Si suspension displays nearly pure SiC.

3.5 SEM and EDS Analysis

Figure 19 shows the SEM images of balsa across three different stages: native, pyrolyzed and SiC forms. As illustrated, the honeycomb structure of the wood is retained throughout and the pores maintain roughly the same size. However, the strut thickness seems to decrease. After SiC formation, the cell walls become so thin to an extent that voids start appearing. This happens because both reactions 1 and 5 work on consuming

amorphous carbon and SiC. As a consequence, the resulting sample expresses an extremely low density (60 kg/m^3) and poor mechanical properties.

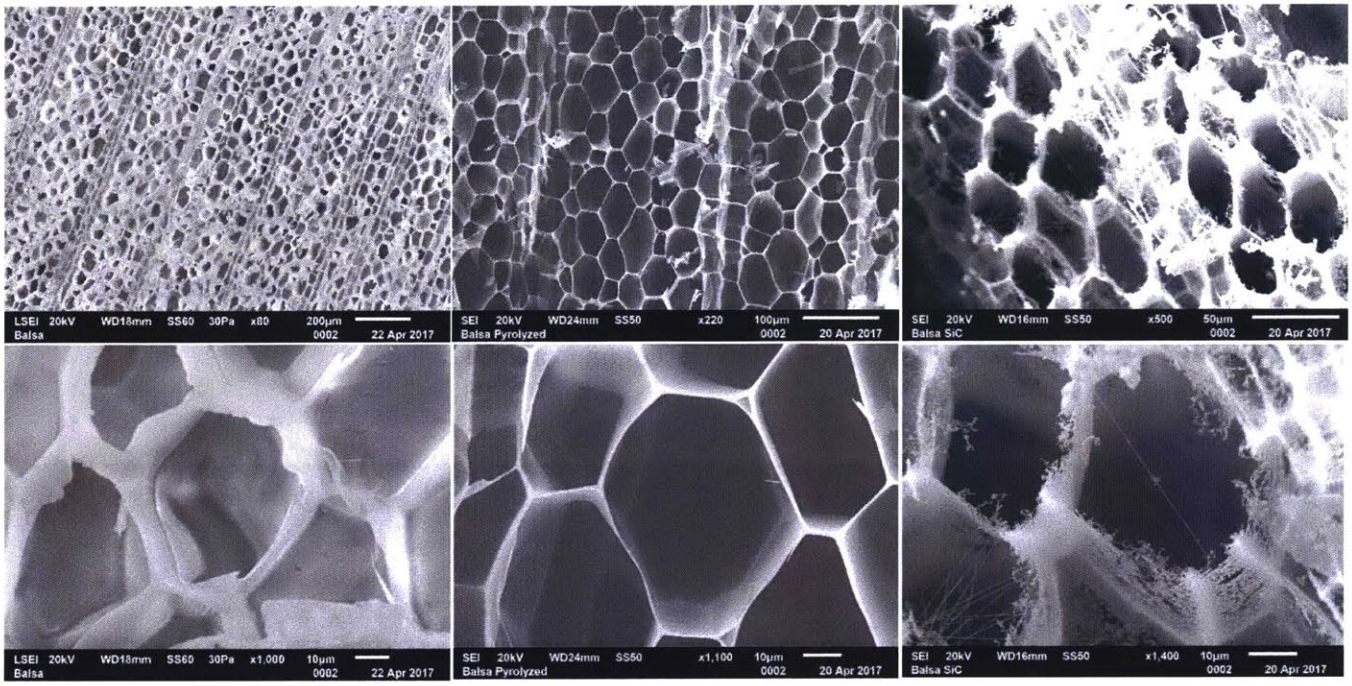

Figure 19: SEM images of balsa in the following states from left to right: native, pyrolyzed and SiC.

Pine, on the other hand, doesn't reveal these voids (Figure 20), which can be attributed to the following. First, pine has a higher density with more carbon supply and better mechanical properties. Second, a lower weight gain percentage was achieved by pine (48.6%) compared with that of balsa (76.8%).

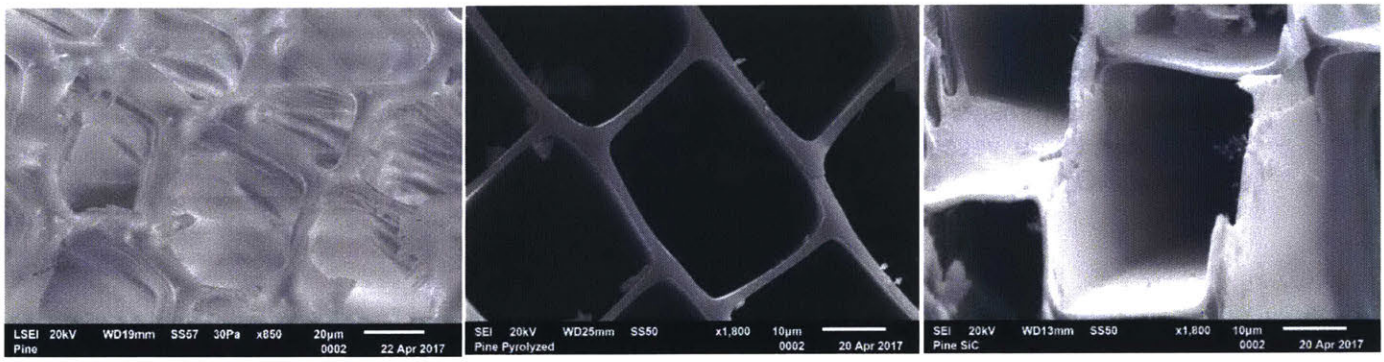

Figure 20: SEM images of pine pore in its native, pyrolyzed and SiC forms from left to right respectively.

Oak's structure over the three different stages is shown in Figure 21. Unlike balsa and pine, oak encompasses large vessels where much of the silica may reside. The bottom-left corner of the SiC image reveals a cylinder of unreacted SiO_2 trapped in one of oak's vessels. Its identity was confirmed via EDS by consisting of no carbon and nearly a 2:1 ratio of oxygen to Si. In addition, formation of SiC whiskers are observed as reported by others. These are the shiny spiky spots on the bottom right image. A zoomed in shot is shown in Figure 21. The whiskers develop according to reaction 7.[39] Since the reactants are gaseous, they likely form in the pores detached from the cell wall.

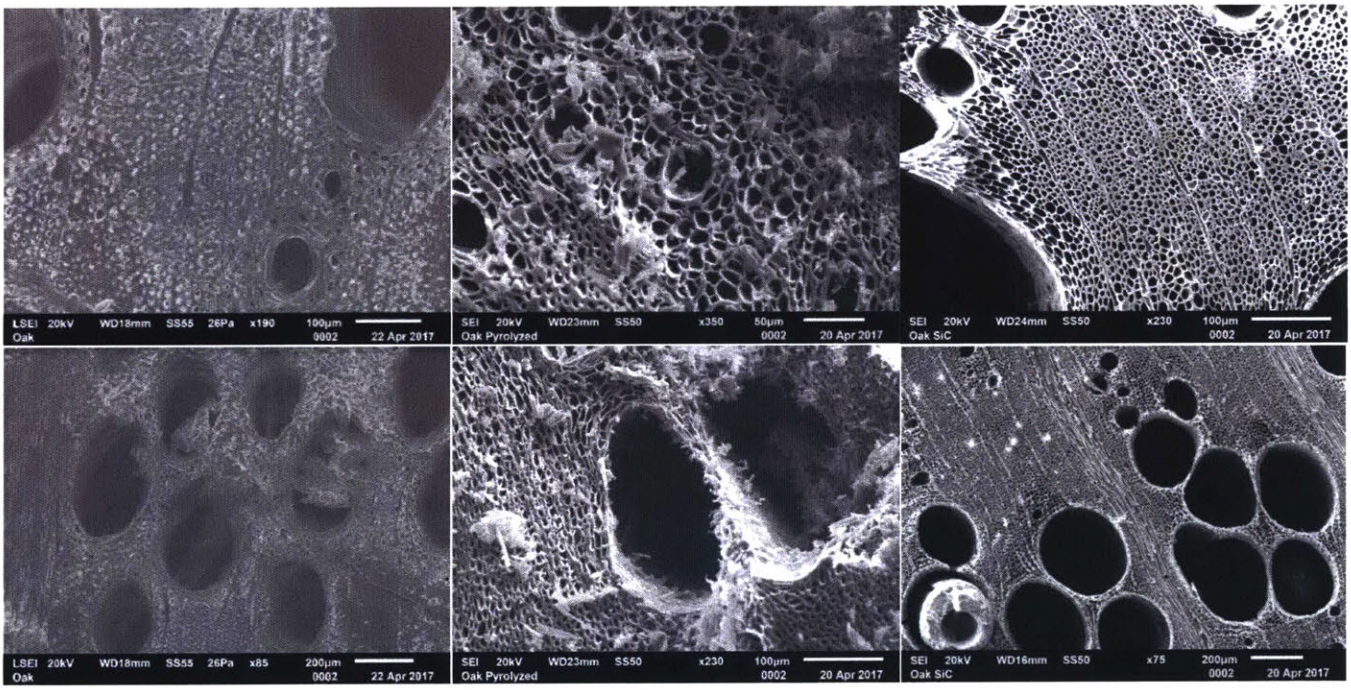

Figure 21: SEM images of oak in its native, pyrolyzed and SiC states from left to right respectively. Large vessels of oak are illustrated in the bottom row, and a cylinder of unreacted SiO_2 is shown in the bottom-right image.

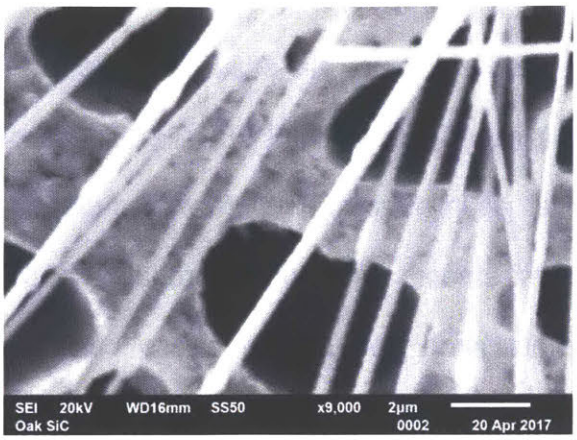

Figure 22: SEM image of SiC whiskers in the oak specimen

$$SiO_{(g)} + 3CO_{(g)} \rightarrow SiC_{(s)} + 2CO_{2(g)} \quad (7)$$

An SEM image of the Si prepared pine SiC specimen cut along the grain is displayed below (Figure 23). In addition, its EDS elemental Si map is shown with the frequency represented by the yellow dots. The map indicates that Si is distributed homogenously over the sample thickness, suggesting that Si was able to diffuse entirely through and react with amorphous carbon. Although the size of the starting Si particles was much bigger than that of SiO_2, successful infiltration and conversion was possible.

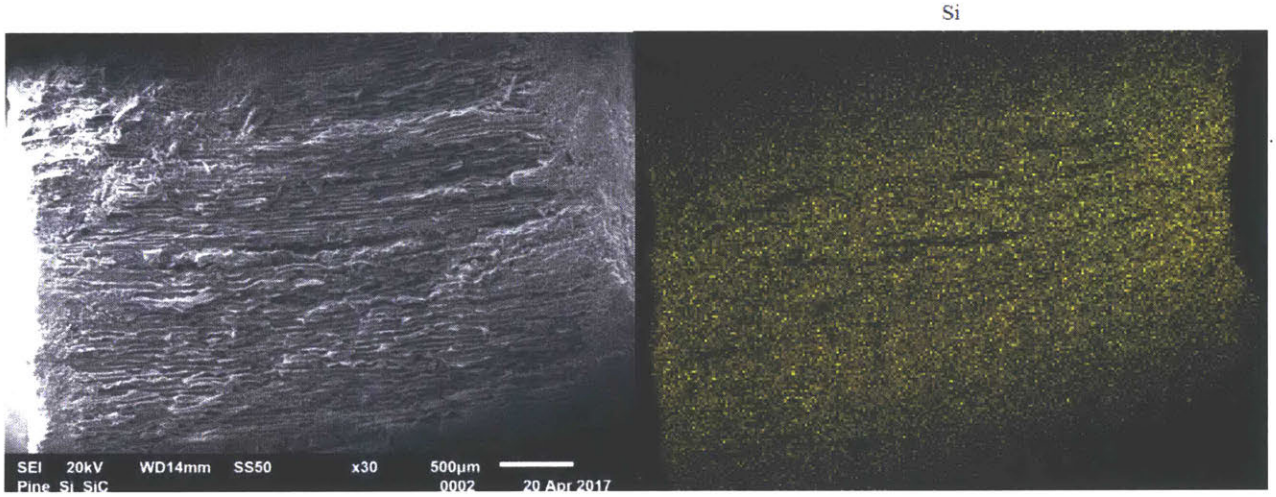

Figure 23: Along the grain SEM image of SiC specimen prepared from infiltrating pine with Si suspension, and corresponding EDS elemental map of Si indicates homogeneous distribution of Si over entire thickness

3.6 Compression Testing Analysis

The plots below represent the stress-strain curves of the SiC samples prepared from balsa, maple and pine (Figure 24 and 25). Testing on oak was not performed because the specimen fell apart after burning off excess carbon. It is important to note that the curves are not smooth and ideal, probably due to sample curvature, misalignment, edge effects and non-uniform stress conditions within the sample. Therefore, minor cracks are observed before yielding.

Balsa shows an atypical curve with no clear signs of elastic failure. After the test, the sample remained intact but lost some of its thickness. The load seemed to have been shattering the surfaces. Thus, the curve is a depiction of elastic deformation, crushing and densification all happening simultaneously. Maple has a clear elastic region followed by a combination of crushing and densification. However, compared with pine, maple has a lower yield strength even though native maple is stronger than native pine. The reason behind that is that, as discussed earlier, maple lost 18.5% percent of its weight after burning off the remaining carbon. This, in turn, diminished a part of maple's structure, thereby, negatively affecting its mechanical properties.

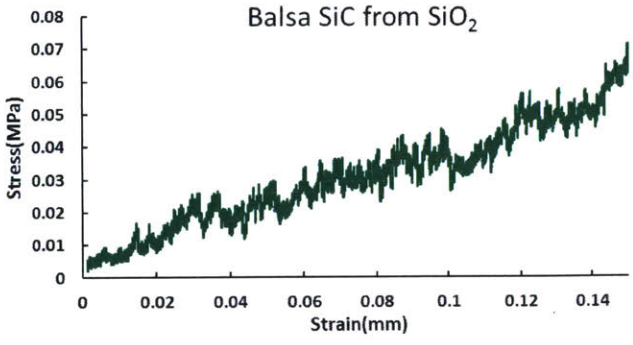

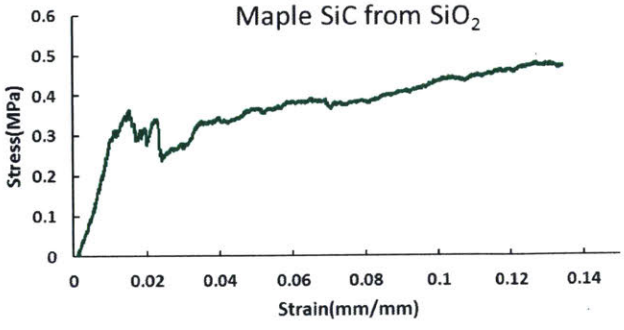

Figure 24: Stress vs strain plots for balsa and maple SiC samples prepared from soaking in colloidal SiO_2 and firing at 1600 °C for 2 h.

The curves below depict the mechanical behavior of biomorphic SiC synthesized via two different methods: from colloidal SiO_2 and from a Si suspension. The latter shows both a higher strength and Young's modulus suggesting the Si suspension technique may produce samples with better mechanical properties.

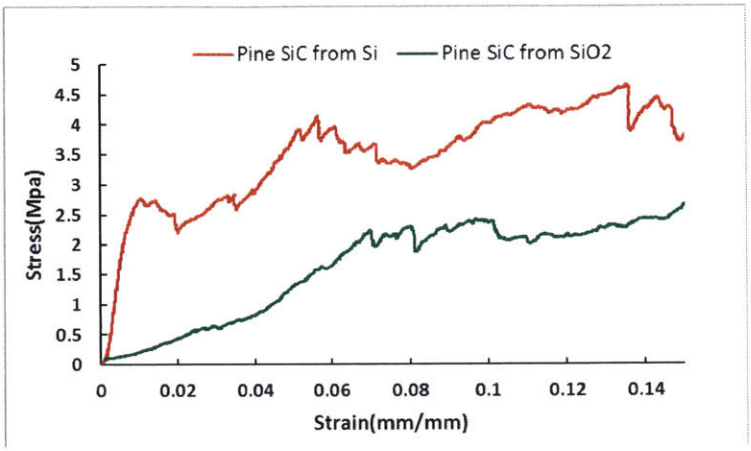

Figure 25: Pine SiC sample prepared from infiltrating with Si suspension shows better mechanical properties than that infiltrated with colloidal SiO_2.

4. Conclusion and Future Work

The goal of this work was to optimize the synthesis process of biomorphic SiC. The approach taken here was to study the state of the art processes employed by others, choose the most viable of them, optimize the technique, and develop a new synthesis route that overcomes the issues involved.

Of the three main methods carried out in literature, infiltration of wood with SiO_2 was considered to be the most efficient and economical compared with the molten Si and chemical vapor infiltration techniques. The most commonly used starting solution is TEOS, and sodium silicate. However, this thesis demonstrates that colloidal silica can be used as a more efficient, cheaper and safer option, ultimately yielding pure biomorphic

SiC. The use of pressure during the infiltration step was also investigated. It was found that applying pressure or vacuum produced more effective weight gains than the lack of either. In addition, for balsa, maple and oak, the use of pressure alone and vacuum followed by pressure yielded roughly the same percent weight gains. Of the four wood types, pine showed superior absorption with its maximum obtained value attained under vacuum followed by pressure. Next, the concentration and amount of SiO_2 solution absorbed proved to be critical in determining the final properties of the specimens. SiO_2 can not only react with carbon to produce SiC, but also with the resulting SiC., This degradation of SiC greatly diminishes the mechanical integrity of the samples. Even though maple absorbed ~3% above its stoichiometric need, 18% of its final weight consisted of unreacted carbon. Both balsa and pine that absorbed 325% and 174% of their weights respectively disintegrated after firing at 1600 °C for 2 h, whereas those that absorbed 76.8% and 48.6% emerged intact. XRD analysis revealed that the resulting samples consisted of nearly pure SiC. Although balsa absorbed more than twice its stoichiometric need, no cristobalite peaks appeared suggesting that excess SiO_2 reacted with SiC, weakening the structure. SEM images captured the honeycomb structure of wood and illustrated that the initial structure of wood is retained after synthesis. The main disadvantage of using SiO_2 is that the nature of the reactions involved generate mechanically weak specimens; SiO_2 requires 3 carbon atoms to produce 1 SiC molecule, and SiO_2 also reacts with SiC.

The new synthesis technique developed in this thesis involves the use of <10 μm sized particles of Si instead of nano-sized SiO_2 particles. Si reacts with only one carbon atom to produce SiC, and unlike SiO_2, Si doesn't consume the resulting SiC. Pine, having

shown to exhibit superior absorption capabilities, was chosen to serve as the template for the reactions. After two infiltration treatments, the sample absorbed 55.6% of its weight, which is ~4% higher than its stoichiometric need, 51.3%. The macro pore size of the wood was demonstrated to allow penetration of Si particles, and the EDS analysis revealed that Si was able to spread homogenously across the entire thickness of the sample. The sample experienced nearly zero weight loss after heat treating at 700 °C in air for 2 h, indicating that no excess carbon was left unreacted. 55.6% weight gain was enough to achieve complete conversion. XRD spectra confirmed the material identity to consist of mainly SiC along with minor contamination, but no Si or SiO_2 peaks present. Finally, mechanical properties were investigated by means of compression testing, and it was found that the pine sample prepared by this technique expressed higher strength and Young's modulus than that prepared using SiO_2, suggesting the great potential of this method to replace existing ones.

Proposed future work includes the following:

- Replication and further optimization of the Si suspension infiltration synthesis process. While a temperature of 1600 °C for 2 h was used, temperatures as low as the melting point of Si (~1400 °C) for less holding times may be adequate to achieve complete conversion. In addition, it is possible to experiment with different starting Si concentrations and investigate whether the required %wt. gain can be obtained after only one infiltration treatment. The effect of using vacuum alone, instead of vacuum followed by pressure, on the %wt. gain can also be studied. The slight curvature of the sides might affect the overall mechanical properties and, therefore, trying to eliminate this deformation may be essential.

- Performing in-depth mechanical, corrosion and temperature tolerance testing. Incorporation of different mechanical assessment techniques such as three-point or four-point bending, in addition to compression testing, may provide a more comprehensive depiction the sample's properties. Inspecting the material's behavior as a function of temperature and different pH conditions may also be relevant.
- Exploring permeability and thermal conductivity. For filtering applications, permeability is a key quality since it directly affects the pressure drop across a filter.[55] By allowing a gas with known viscosity and velocity to flow through a specimen, the pressure drop can be measured via Darcy's law.[27] Also, since biomorphic SiC has potential applications at high temperatures, it is important to understand its thermal properties, which can be determined both experimentally and computationally as others have examined them. [24,56]

5. References

1. Studart, A. R., Gonzenbach, U. T., Tervoort, E. & Gauckler, L. J. Processing routes to macroporous ceramics: A review. in *Journal of the American Ceramic Society* **89,** 1771–1789 (Blackwell Publishing Inc, 2006).

2. Lefebvre, L.-P., Banhart, J. & Dunand, D. C. Porous Metals and Metallic Foams: Current Status and Recent Developments. *Adv. Eng. Mater.* **10,** 775–787 (2008).

3. Meille, S., Lombardi, M., Chevalier, J. & Montanaro, L. Mechanical properties of porous ceramics in compression: On the transition between elastic, brittle, and cellular behavior. *J. Eur. Ceram. Soc.* **32,** 3959–3967 (2012).

4. Sieber, H., Hoffmann, C., Kaindl, A. & Greil, P. Biomorphic Cellular Ceramics. *Adv. Eng. Mater.* **2,** 105–109 (2000).

5. Arellano-López, a. R. *et al.* Biomorphic SiC : A New Engineering Ceramic Material. *Int. J. Appl. Ceram. Technol.* **67,** 56–67 (2004).

6. Lohr, J. *et al.* Production process of wood-based materials for SiC Ceramics. *Eur. J. Wood Wood Prod.* **71,** 417–428 (2013).

7. Eom, J.-H., Kim, Y.-W. & Raju, S. Processing and properties of macroporous silicon carbide ceramics: A review. *Integr. Med. Res.* **1,** 220–242 (2013).

8. Qian, J.-M., Jin, Z.-H. & Wang, X.-W. Porous SiC ceramics fabricated by reactive infiltration of gaseous silicon into charcoal. *Ceram. Int.* **30,** 947–951 (2004).

9. Elias, H., Hyie, K. M., Kalam, A. & Rahman, N. A. Conversion of biomorphic silicon carbide from wood powders carbon template. in *AIP Conference Proceedings* 60004 (AIP Publishing LLCAIP Publishing, 2016). doi:10.1063/1.4965112

10. Kaul, V. S., Faber, K. T., Sepúlveda, R., de Arellano López, A. R. & Martínez-Fernández, J. Precursor selection and its role in the mechanical properties of porous SiC derived from wood. *Mater. Sci. Eng. A* **428,** 225–232 (2006).

11. Singh, M. & Yee, B.-M. Reactive processing of environmentally conscious,

biomorphic ceramics from natural wood precursors. *J. Eur. Ceram. Soc.* **24,** 209–217 (2004).

12. Locs, J., Berzina-Cimdina, L., Zhurinsh, A. & Loca, D. Optimized vacuum/pressure sol impregnation processing of wood for the synthesis of porous, biomorphic SiC ceramics. *J. Eur. Ceram. Soc.* **29,** 1513–1519 (2009).

13. Singh, M. & Salem, J. . Mechanical properties and microstructure of biomorphic silicon carbide ceramics fabricated from wood precursors. *J. Eur. Ceram. Soc.* **22,** 2709–2717 (2002).

14. Greil, P., Lifka, T. & Kaindl, A. Biomorphic Cellular Silicon Carbide Ceramics from Wood: I. Processing and Microstructure. *J. Eur. Ceram. Soc.* **18,** 1961–1973 (1998).

15. Varela-Feria, F. M., Martínez-Fernández, J., De Arellano-López, A. R. & Singh, M. Low density biomorphic silicon carbide: Microstructure and mechanical properties. *J. Eur. Ceram. Soc.* **22,** 2719–2725 (2002).

16. Muñoz, A., Martínez Fernández, J. & Singh, M. High temperature compressive mechanical behavior of joined biomorphic silicon carbide ceramics. *J. Eur. Ceram. Soc.* **22,** 2727–2733 (2002).

17. Qiao, G., Ma, R., Cai, N., Zhang, C. & Jin, Z. Mechanical properties and microstructure of Si/SiC materials derived from native wood. *Mater. Sci. Eng. A* **323,** 301–305 (2002).

18. González, P. *et al.* New biomorphic SiC ceramics coated with bioactive glass for biomedical applications. *Biomaterials* **24,** 4827–4832 (2003).

19. Zollfrank, C. & Sieber, H. Microstructure and phase morphology of wood derived biomorphous SiSiC-ceramics. *J. Eur. Ceram. Soc.* **24,** 495–506 (2004).

20. Esposito, L., Sciti, D., Piancastelli, A. & Bellosi, A. Microstructure and properties of porous β-SiC templated from soft woods. *J. Eur. Ceram. Soc.* **24,** 533–540 (2004).

21. de Arellano-López, A. R. *et al.* Erosion and strength degradation of biomorphic SiC. *J. Eur. Ceram. Soc.* **24,** 861–870 (2004).

22. Yukhymchuk, V. O. *et al.* Biomorphous SiC ceramics prepared from cork oak as precursor. *J. Phys. Chem. Solids* **91,** 145–151 (2016).

23. Bautista, M. A., Cancapa, J. Q., Fernandez, J. M., Rodríguez, M. A. & Singh, M. Microstructural and mechanical evaluation of porous biomorphic silicon carbide for high temperature filtering applications. *J. Eur. Ceram. Soc.* **31,** 1325–1332 (2011).

24. Pappacena, K. E., Faber, K. T., Wang, H. & Porter, W. D. Thermal conductivity of porous silicon carbide derived from wood precursors. *J. Am. Ceram. Soc.* **90,** 2855–2862 (2007).

25. Wang, W., Hou, G., Wang, B. & Deng, S. Preparation of biomorphic silicon carbide–mullite ceramics using molten salt synthesis. *Mater. Chem. Phys.* **147,** 198–203 (2014).

26. Maity, A. *et al.* Microstructural and mechanical characterisation of biomorphic SiC ceramics synthesised from coir fibreboard preform. *Mater. Sci. Eng. A* **565,** 72–79 (2013).

27. Gómez-Martín, A., Orihuela, M. P., Becerra, J. A., Martínez-Fernández, J. & Ramírez-Rico, J. Permeability and mechanical integrity of porous biomorphic SiC ceramics for application as hot-gas filters. *Mater. Des.* **107,** 450–460 (2016).

28. Material Safety Data Sheet for: Silicon Tetrafluoride (SiF 4) Section 1: Chemical Product and Company Identification.

29. Torres-Raya, C. *et al.* Fabrication, chemical etching, and compressive strength of porous biomimetic SiC for medical implants. (2017). doi:10.1557/JMR.2008.0392

30. Sieber, H., Vogli, E. & Greil, P. Biomorphic SiC-ceramic manufactured by gas phase infiltration of pine wood. *25th Annu. Conf. Compos. Adv. Ceram. Mater. Struct. B* **22,** 109–116\r642 (2001).

31. Vogli, E., Sieber, H. & Greil, P. Biomorphic SiC-ceramic prepared by Si-vapor phase infiltration of wood. *J. Eur. Ceram. Soc.* **22,** 2663–2668 (2002).

32. Qian, J.-M., Wang, J.-P. & Jin, Z.-H. Preparation and properties of porous microcellular SiC ceramics by reactive infiltration of Si vapor into carbonized basswood. *Mater. Chem. Phys.* **82,** 648–653 (2003).

33. Vogli, E. *et al.* Conversion of Oak to Cellular Silicon Carbide Ceramic by Gas-Phase Reaction with Silicon Monoxide. *J. Am. Ceram. Soc.* **84,** 1236–1240 (2004).

34. Streitwieser, D. A., Popovska, N., Gerhard, H. & Emig, G. Application of the chemical vapor infiltration and reaction (CVI-R) technique for the preparation of highly porous biomorphic SiC ceramics derived from paper. *J. Eur. Ceram. Soc.* **25,** 817–828 (2005).

35. Streitwieser, D. A., Popovska, N. & Gerhard, H. Optimization of the ceramization process for the production of three-dimensional biomorphic porous SiC ceramics by chemical vapor infiltration (CVI). *J. Eur. Ceram. Soc.* **26,** 2381–2387 (2006).

36. Dhiman, R., Petrunin, V., Rana, K. & Morgen, P. Conversion of wooden structures into porous SiC with shape memory synthesis. (2011). doi:10.1016/j.ceramint.2011.05.124

37. Klinger, R. *et al.* Wood-derived porous ceramics via infiltration of SiO2-Sol and carbothermal reduction. *Holzforschung* **57,** 440–446 (2003).

38. Ota, T. *et al.* Biomemeic process for producing SiC 'wood'. *Journal of the American Ceramic Society* **78,** 3409–3411 (1995).

39. Qian, J., Wang, J. & Jin, Z. Preparation of biomorphic SiC ceramic by carbothermal reduction of oak wood charcoal. *Mater. Sci. Eng. A* **371,** 229–235 (2004).

40. Herzog, A., Klingner, R., Vogt, U. & Graule, T. Wood-Derived Porous SiC Ceramics by Sol Infiltration and Carbothermal Reduction. *J. Am. Ceram. Soc.* **87,** 784–793 (2004).

41. Qian, J.-M., Wang, J.-P., Qiao, G.-J. & Jin, Z.-H. Preparation of porous SiC ceramic with a woodlike microstructure by sol-gel and carbothermal reduction processing. *J. Eur. Ceram. Soc.* **24,** 3251–3259 (2004).

42. Shin, Y., Wang, C. & Exarhos, G. J. Synthesis of SiC ceramics by the carbothermal reduction of mineralized wood with silica. *Adv. Mater.* **17,** 73–77 (2005).

43. Qian, J.-M. & Jin, Z.-H. Preparation and characterization of porous, biomorphic SiC ceramic with hybrid pore structure. *J. Eur. Ceram. Soc.* **26,** 1311–1316 (2006).

44. Vyshnyakova, K., Yushin, G., Pereselentseva, L. & Gogotsi, Y. Formation of Porous SiC Ceramics by Pyrolysis of Wood Impregnated with Silica. *Int. J. Appl. Ceram. Technol* **3,** 485–490 (2006).

45. Locs, J., Berzina-Cimdina, L., Zhurinsh, A. & Loca, D. Effect of processing on the microstructure and crystalline phase composition of wood derived porous SiC ceramics. *J. Eur. Ceram. Soc.* **31,** 183–188 (2011).

46. Shin, Y. & Exarhos, G. J. Conversion of cellulose materials into nanostructured ceramics by biomineralization. *Cellulose* **14,** 269–279 (2007).

47. Hołowacz, I., Podbielska, H. & Bauer, J. Viscosity, surface tension and refractive index of tetraethylorthosilicate-based sol-gel materials depending on ethanol content. *Opt. Appl.* **XXXV,** (2005).

48. Nagao, D. *et al.* Particle formation in the hydrolysis of tetraethyl orthosilicate in pH buffer solution. *J. Colloid Interface Sci.* **279,** 143–149 (2004).

49. Yang, X., Zhu, W. & Yang, Q. The Viscosity Properties of Sodium Silicate Solutions. *J Solut. Chem* **37,** 73–83 (2008).

50. Safety Data Sheet. (2016).

51. Silicate, S. Safety Data Sheet. (2014).

52. LUDOX® TM-50 colloidal silica 50 wt. % suspension in H2O | Sigma-Aldrich.

Available at: http://www.sigmaaldrich.com/catalog/product/aldrich/420778?lang=en&region=US. (Accessed: 1st May 2017)

53. Gibson, L. J. The hierarchical structure and mechanics of plant materials. *J. R. Soc. Interface* **9,** 2749–66 (2012).

54. Sinha, S., Jhalani, A., Ravi, M. R. & Ray, A. Modelling of Pyrolysis in Wood: A Review.

55. Eom, J.-H., Kim, Y.-W. & Song, I.-H. Effects of the initial α-SiC content on the microstructure, mechanical properties, and permeability of macroporous silicon carbide ceramics. *J. Eur. Ceram. Soc.* **32,** 1283–1290 (2012).

56. Sulistyo, J. *et al.* Electrical and thermal conductivities of porous SiC/SiO2/C composites with different morphology from carbonized wood. *J. Mater. Sci.* **45,** 1107–1116 (2010).